ELSEVIER

NeuroImage

www.elsevier.com/locate/ynimg
NeuroImage 30 (2006) 835 – 846

Investigating direct detection of axon firing in the adult human optic nerve using MRI

Li Sze Chow,[a,b] Greg G. Cook,[a] Elspeth Whitby,[b] and Martyn N.J. Paley[b,*]

[a]*Department of Electronic and Electrical Engineering, University of Sheffield, Mappin Street, S1 3JD Sheffield, UK*
[b]*Section of Academic Radiology, University of Sheffield, Royal Hallamshire Hospital, Glossop Road, S10 2JF Sheffield, UK*

Received 7 July 2005; revised 6 October 2005; accepted 10 October 2005
Available online 20 December 2005

The aim of this study was to directly detect spectral components of the magnetic fields of ionic currents caused by firing of the axons in the optic nerve in response to visual strobe stimulation. The magnetic field parallel to the main B_0 field can potentially alter the local phase and magnitude of the MR signal which can cause signal loss due to intravoxel dephasing. Measured frequency spectra showed evidence of the strobe stimulus localized to regions containing the optic nerve, not thought to be due to motion artifacts, in 30 out of 52 experiments in 5 adult human subjects. The effect was (0.15 ± 0.05)% of the mean magnitude equilibrium signal from the voxel in the frequency range 0.7–3.3 Hz, corresponding to an estimated field of (1.2 ± 0.4) nT, at an echo time of TE = 32.4 ms using a 1.5 T MRI scanner. Only 1 of 12 phase image experiments showed effects. These findings provide preliminary evidence for direct detection of axonal firing in the optic nerve.

Keywords: Axonal firing; Direct MR axonal detection; Direct MR neuronal detection; Optic nerve

Introduction

There have been many studies and recent advances in mapping human brain activity. Magnetoencephalography (MEG) and electroencephalography (EEG) are based on the detection of the electrophysiological processes that constitute brain function. Single photon emission computed tomography (SPECT), positron emission tomography (PET) and functional magnetic resonance imaging (fMRI) all detect hemodynamic and metabolic changes associated with brain function (Ogawa et al., 1990; Hennig et al., 2003; Logothethis et al., 2001; Raichle, 2001).

fMRI detects neuronal activity based on the changes in blood oxygen level dependent (BOLD) contrast, which are caused by the effects of neuronal activity on localized brain blood flow, blood volume and oxygenation. There are some limitations on this indirect detection of neuronal activity since both the temporal and spatial resolutions of fMRI are constrained by the slow cerebral hemodynamic response and the complex vascular geometry (rather than inherent limitations of MR imaging). Temporal resolution of the order of 1 s and spatial resolution on the order of 1 mm have been achieved. However, changes in blood flow and blood volume may have a spatial extent that is significantly larger than the actual area of activation, and the relationship between the BOLD response and the underlying neuronal activity is not fully understood.

MEG and EEG measure electromagnetic signals produced by neuronal populations. MEG measures extracranial magnetic fields using Superconducting Quantum Interference Devices (SQUIDs), whereas EEG measures electric potentials on the scalp using electrodes. Both techniques provide excellent temporal resolution, of the order of milliseconds, but poor spatial resolution. By using MEG, spontaneous and evoked magnetic fields measured on the scalp, at a distance of about 2–4 cm from the current source, are of the order of 10^{-12} T and 10^{-13} T respectively (Hamalainen et al., 1993). If the source of these magnetic fields is modeled as a current dipole, the magnetic fields are expected to be much larger near the current source because they are inversely proportional to the square of the distance. There has been a suggestion that the fields from axons may actually fall off as magnetic quadrupoles (i.e. as the inverse cube of the distance) which would mean the fields detected from axons in the optic nerve by MEG would be much weaker than those from neuronal dipole sources in the cortex (Hamalainen et al., 1993). However, this would not affect the MRI measurement where the spins being modulated give rise to the signal directly. This could explain why signals from the optic nerve are not routinely observed with MEG but could potentially be seen by MRI. At an MRI distance scale of 1–2 mm, calculations assuming a conventional dipolar field fall-off suggest local magnetic fields from neurons of the order of 10^{-9} T for spontaneous activity such as alpha waves and 10^{-10} T for

* Corresponding author. Fax: +44 114 2724760.
E-mail address: m.n.paley@shef.ac.uk (M.N.J. Paley).
Available online on ScienceDirect (www.sciencedirect.com).

1053-8119/$ - see front matter © 2005 Elsevier Inc. All rights reserved.
doi:10.1016/j.neuroimage.2005.10.024

evoked activity. For MEG to detect a field from a quadrupolar source, it would need to be of the order of 10^{-8} T to 10^{-7} T locally.

Individually, the switching ion channels give rise to minute currents of the order of 10^{-12} A, as measured using patch clamp experiments, but the summed current from all the ion channels in an axon can be as high as 10^{-9} A, (Purves et al., 2001). Assuming a wire model for the field B_{ax} and the radius of the axon, $r = 0.5$ μm yields $B_{ax} = 4\pi 10^{-7}\ I/2\pi r = 4 \times 10^{-10}$ T. This is consistent with the maximum local field estimates from MEG stated above.

There has been great interest in non-invasively imaging currents in the human body since the original development of applied potential tomography in the early 1980s which used extrinsically applied currents to visualize current paths in the body directly (Barber and Brown, 1983). The first papers to attempt to measure current from externally applied currents using magnetic resonance imaging required rotation of the sample relative to B_0 and extensive image processing in order to fully quantify the distribution (Joy et al., 1989; Scott et al., 1992). A later development used rotating frame excitation to avoid inconvenient physical rotations of the sample (Scott et al., 1995). However, these pioneering studies were not specifically aimed at detecting weak neuronal currents in vivo.

Several methods have been introduced recently to detect transient magnetic field changes using MRI, which might be feasible for mapping neuronal activity. These have focused less on the quantitative aspects of current measurement and more on investigating the temporal modulation of the local magnetic field by weak fluctuating quasi-periodic current sources. A number of phantom studies have demonstrated that it is in fact feasible to measure magnetic fields similar to those expected from neuronal firing using either magnitude or phase MR images (Bodurka et al., 1999; Bodurka and Bandettini, 2002; Kamei et al., 1999; Konn, 2003; Konn et al., 2003; Yang et al., 2003). However, in vivo, the exact mechanism and expected magnitude of possible signal changes are still a source of debate. Recent in vivo studies have investigated motor paradigms (Kamei et al., 1999), visuo-motor tasks (Xiong et al., 2003), spontaneous alpha waves (Konn et al., 2004), strobe stimulation of the optic nerve (Chow et al., 2004), electrical activity in epilepsy seizures (Liston et al., 2004) and a sophisticated visual stimulation paradigm to acquire both BOLD and neuronal detection measurements in a single scan (Chu et al., 2004). Although a number of both positive and negative claims have been made regarding the capability of MR to perform direct neuronal detection, the field is still in a preliminary investigation phase, and further studies in different anatomical regions, which may be more conducive to direct detection, are warranted.

The study reported here used a short TR gradient echo EPI sequence with intermediate echo time at 1.5 T to perform real-time imaging of the optic nerve during visual stimulation by stroboscopic illumination for a range of frequencies up to 3.3 Hz. Since there are about one million highly directed axons forming the optic nerve (Mikelberg et al., 1989) which fill the imaging voxel in a symmetrical distribution (see Fig. 1b), any overall phase variation would be expected to average out completely (Konn et al., 2004). However, the multiple microscopic axonal sources of field inhomogeneity should still cause a signal loss on magnitude images due to intravoxel dephasing, which is explained in the Methods section. If the SNR is made sufficiently high, then repetitive modulation effects should be detected through Fourier transformation even though the resulting fractional changes are very small. For these reasons, we chose to use magnitude images in this study, although phase images were also analyzed for comparison in a subset of cases.

Methods

Background theory

Neurons use a combination of graded, local potential changes and brief, actively propagated action potentials. Local potentials

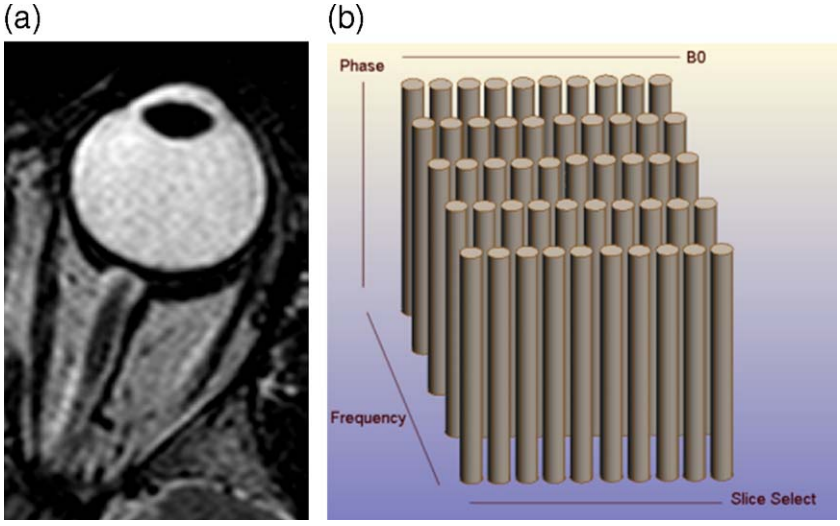

Fig. 1. (a) High resolution fast spin echo image of the optic nerve and orbit acquired using a 6-channel SENSE head coil (3 T Intera, Philips, NL) showing the parallel axons within the dural sheath to illustrate the highly symmetrical anatomy. The optic nerve actually forms part of the CNS and is continuous with the brain. Sequence parameters were TR = 3000 ms, TE = 120 ms, in-plane resolution = 0.45 mm, SLT = 1 mm, NEX = 1, ETL = 15. (b) Schematic diagram showing the location of the optic nerve axons relative to B_0 and the image encoding axes. Experiments were also performed with the phase and frequency directions swapped to assess motion effects. The optic nerve contains 9.26×10^5 parallel axons with an average diameter of 0.72 μm packed into an extended cylinder of diameter ~3000 μm.

often develop and decay relatively slowly and reflect extended connections, whereas action potentials, also known as spikes or nerve impulses, actively propagate over long distances. Action potentials are followed by a brief refractory period typically lasting several milliseconds, hence, the absolute upper limit on action potential frequency is a few hundred hertz. In the optic nerve, under photopic illumination, synchronized data bursts with durations from tens of milliseconds up to hundreds of milliseconds are observed even for a brief duration flash (Shimada et al., 2001; Kolb et al., 2002; Sterling and Demb, 2004). Refractory periods help ensure that action potentials are propagated in only one direction. Action potentials typically are initiated at a trigger zone in the axon near the cell body and then spread antidromically and passively into the inexcitable cell body and propagate orthodromically down the axon (Kandel et al., 2000; Nolte, 2002).

Axonal (ionic) current is not carried by electrons but rather by the movement of ions, driven by the energy stored in ionic concentration gradients and controlled by molecular switches. On excitation by an action potential, the conductance of the sodium ion channels increases dramatically, and Na^+ ions flow in through the axon membrane for about 1 ms and perpendicular to the long axis of the axons at the Nodes of Ranvier (which are 1–2 μm intervals in the myelination of the axon found approximately every 1–2 mm). Current then flows passively down the axon to the next node at a rate of between 6 and 15 mm/ms dependent on the axonal diameter. K^+ ions then flow out, after a short delay, resulting in a slight negative undershoot of the net trans-membrane potential. Action potentials repeat every few milliseconds for an extended period dependent on the intensity, frequency, color and retinal position of the stimulation (Kandel et al., 2000; Nolte, 2002).

These currents induce transient magnetic fields, and the components that are parallel to the main B_0 field can locally alter the precession rate of water protons and hence alter the phase and magnitude of the MR signal. In this study, the optic nerve was chosen for in vivo experiments because the axons are conveniently perpendicular to the B_0 field (Figs. 1a and b), and therefore components of their magnetic fields will lie in the B_0 field direction. The action potentials are initiated from ganglion cells in the retina, and bursts of data are expected at the stimulus frequency.

The diffusion coefficient D of the optic nerve is $\sim 10^{-9}$ m^2 s^{-1} (Wheeler-Kingshott et al., 2002). Assuming the axonal fields are active over a range r of ~5 μm, the diffusion correlation time $\tau_D = r^2/D$ is ~0.025 s, which is in the intermediate to static dephasing regime. This assumption is required to see T2* changes due to field modulation as they would disappear in the motional narrowing regime. The axonal modulating signal as a function of echo time is given by Kennan et al. (1994)

$$S(\mathrm{TE}) = S_0 < e^{-i\phi_j} >_{\mathrm{TE}} = S_0 < e^{-i\gamma\delta B_{\mathrm{ax}}\mathrm{TE}} > \quad (1)$$

where ϕ_j are the phase shifts introduced by the axonal fields δB_{ax} at TE. The axonal field distribution could be modeled in a number of ways. A simple model for the generation of the averaged magnetic field in a voxel $\delta B_{\mathrm{ax}}(t)$ could be to assume the axons to be a bundle of a million or so 'micro-wires', each carrying a current which generates a component of the field. Alternatively, the strongest modulation may be due to the moving ionic current sources themselves, which are essentially randomly located within the voxel and have a much smaller radius ($\sim 10^{-10}$ m) than the axons, thus producing a much higher local modulating field. Assuming the fields within the voxel produce a Lorentzian distribution leads to a linear dependence on the axonal fields and echo time (Brown, 1961; Kennan et al., 1994). The maximum magnitude percentage contrast change from the voxel as a function of echo time TE is then given by

$$\%|\Delta S/S_{\mathrm{eq}}| = 100\left[1 - e^{-\mathrm{TE}(\mathrm{R2}^*_{\mathrm{ax}} - \mathrm{R2}^*)}\right] \quad (2)$$

where R2* is the transverse relaxation rate of the optic nerve in the absence of stimulation (assumed to be similar to white matter ~11.1 s^{-1} at 1.5 T) and $\mathrm{R2}^*_{\mathrm{ax}}$ is given by

$$\mathrm{R2}^*_{\mathrm{ax}} = \mathrm{R2}^* + \gamma|\delta B_{\mathrm{ax}}(t)| \quad (3)$$

where $\gamma|\delta\ B_{\mathrm{ax}}(t)|(s^{-1})$ is the average frequency change introduced by the transient current within the axons contained in the voxel, generated from an envelope of action potentials assumed to fire throughout data collection.

Phantom studies

A small cylindrical water phantom (33 mm diameter, 15 mm height) was wound with four turns of copper wire fed from an analogue signal generator (Thurlby-Thandar Ltd., Huntingdon, UK), with either sinusoidal or square wave currents between 2.7 μA and 33 μA at various frequencies and calibrated using an oscilloscope (TDS5052, Tektronix, USA). The coil axis was aligned parallel to the B_0 field.

Acquisition methodology

All experiments were performed on a 1.5 T Infinion MR system (Philips Medical Systems Inc., Cleveland, OH). A 10 cm diameter surface coil was used for imaging a single optic nerve with high SNR and a 28 cm quadrature head coil for comparison of effects in both optic nerves. Gradient Echo-Echo Planar Imaging (GE-EPI) was used to acquire magnitude images and, in a subset, complex data for offline reconstruction of magnitude and phase images. Three sets of scanning parameters were used as shown in Table 1. The common parameters were: image matrix = 80 × 80, NEX = 1, flip angle (FA) = 90°, orientation = transverse, phase direction = AP or LR, number of frames = 500. Fat saturation was applied for the in vivo experiments to remove signal from retro-orbital fat. An echo time of 32.4 ms was used for most experiments, but a range of echo times from 30 to 78 ms was used in a subset of experiments, which all provided high resolution, high SNR images.

Imaging of the optic nerve was repeated over multiple imaging sessions in five healthy adult human subjects. Four males and one female with an age range of 25–50 years and with normal eyesight in both eyes were studied. Corrective glasses for minor focusing problems were not worn in the magnet due to the possibility of induced eddy currents in the metallic frames. A total of 40 experiments were performed using magnitude images only, and 12

Table 1
Scan parameters for the phantom and in vivo experiments

Scan parameters	(a) Phantom/In vivo	(b) In vivo	(c) In vivo
TR (ms)	132/154	158/172	208/264
TE (ms)	30	32.4	32.4/40/50/78
FOV (mm)	300	240	240
Slice thickness (mm)	5/8	5	5

additional experiments used complex data for offline reconstruction of magnitude and phase images. A foam head mould and Velcro strap were used to ensure that motion of the subject's head was minimized during imaging. Fig. 1b shows a schematic illustration of the optic nerve axon positioning relative to the image voxel. The image plane was carefully selected to include both optic nerves extending from the orbit to the optic chiasm. If the optic nerves were more than a few degrees away from the axial plane, then the head was repositioned so that the nerve was perpendicular to B_0 in order to generate maximum modulation effects.

In vivo experiments were repeated at different strobe light frequencies (0.7–3.3 Hz) for each subject. Heartbeat and respiration rates were measured for each subject before and after image acquisition. The strobe light frequency was chosen to be as far away as possible from the heartbeat and respiration rate and their harmonics as measured before imaging. Subjects were trained not to move their eyes or blink during the relatively short time course of the experiments (<132 s for TR 264 ms) by fixation on a specific point on the magnet bore liner. Subjects were also dark-adapted for 15 min before the visual stimulus experiments started during which time the control experiments took place, with either opened or closed eyes. To assess possible stimulus-related motion artifacts, in vivo experiments were performed as the subjects blinked their eyes at a regular self-paced frequency during imaging, both with and without strobe stimulation.

The spectrum from the strobe light (Model 250, Soundlab, UK) was measured using an optical spectrometer (Ocean Optics, FL) and had a peak output wavelength at 480 nm (within the range of blue light). The strobe light was placed ~3 m away from a subject's eyeballs and observed as a diffuse reflection from the magnet bore liner immediately above the subject's eyes in a darkened room. When the surface coil was used, it was placed along the side of the head parallel to one of the optic nerves, with the side chosen at random. Prior to in vivo experiments, images of a 19 cm cylindrical phantom were acquired using both the surface coil and head coil to ensure that there was no direct electromagnetic interference from the strobe light. All in vivo imaging studies were performed in accordance with local ethical guidelines for MR and with informed written consent.

Image processing and data analysis

Images were processed with software written in-house using MATLAB (The Mathworks Inc., Natick, MA). The first 10 frames were discarded to eliminate effects of the approach to steady state. In a subset of in vivo experiments, complex data were used for offline reconstruction of magnitude and phase images for comparison with the real-time magnitude images. A mean magnitude voxel value (and a mean phase value in a subset of experiments) from a 2 × 2 voxel ROI anatomically located in the optic nerve and a central voxel in the solenoid modulated cylindrical water phantom were used to create a 1D time series from successive frames, which was then Fourier transformed. As the expected fast frequency response of the optic nerve to stimulation was not known a priori, it was decided to investigate the full frequency spectrum from all the ROIs rather than perform a correlation analysis at the single chosen stimulus frequency as is usual for fMRI studies. This also allowed the respiratory and cardiac frequencies and their associated harmonics to be clearly observed as potential sources of artifact, a problem which is generally overlooked in conventional fMRI analysis. The optic nerve occupied relatively few ROIs at the spatial resolution used for the study, so this could be achieved relatively quickly. The temporal standard deviation (TSD) of the time series was calculated, and 2D frequency maps were obtained by displaying a particular frequency component of the Fourier transformed time series for voxels in a wider ROI. Statistical significance was assessed by comparing an anatomically defined region of interest containing the optic nerve with and without stimulation using a pixel-by-pixel Student's t test with a Bonferroni correction on the frequency maps.

The strobe stimulus was not synchronized to the scanner to ensure that the entire modulating waveform from the axonal firing response was sampled repeatedly throughout the time series (Josephs and Henson, 1999). This meant that it was not possible to extract an exact stimulus synchronized averaged time series. However, an approximate averaged time series with a known number of strobe flashes could be obtained by careful estimation of the repeating pattern of strobe flashes by comparing the period of a flash with the TR and then estimating the number of time frames required for averaging.

To ensure that no significant motion had occurred during acquisition of the time series, a 2D autocorrelation was computed between the first and successive frames of subsets of the image containing only the optic nerve (MATLAB, *normxcorr2* function). Motion was then estimated from the peak position of the autocorrelation function. Experiments with deliberate motion of the eyes or blinking were performed to assess the level of artifact produced. Due to the small size of the optic nerve, image interpolation by a factor of 4 was applied before the 2D autocorrelation. Data sets with any significant motion components were not analyzed further.

Results

Simulation

Calculations of the in vivo percentage signal changes due to the additional relaxation process are presented in Fig. 9 for a range of effective δB_{ax} fields from 1.0×10^{-10} T to 2.0×10^{-9} T which correspond to published data for physiological, spontaneous or evoked responses for a range of echo times.

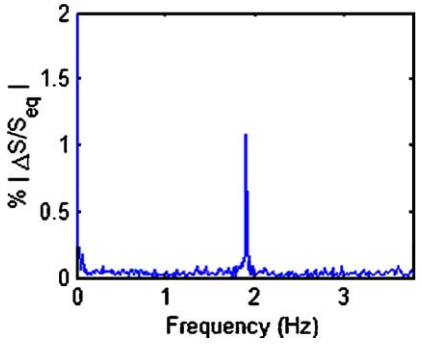

Fig. 2. Measured EPI frequency spectra for the central voxel of the solenoid modulated cylindrical water phantom (voxel size 2.3 × 2.3 × 5 mm^3) obtained from offline reconstructed magnitude images with 1.8 Hz sinusoidal current flowing through the surrounding solenoid modulating coil, producing a calculated local RMS magnetic field of 7.2×10^{-9} T.

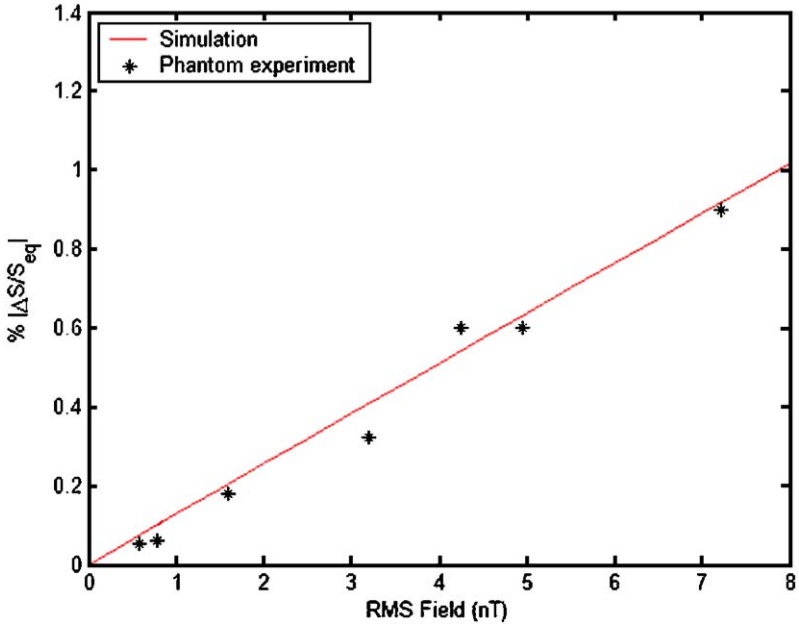

Fig. 3. Measurements from the solenoid modulated cylindrical phantom with different modulating fields plotted against the predicted values from the linear model. The minimum measured RMS field was 5.7×10^{-10} T at an SNR of 2:1.

Phantom experiments

The magnitude spectrum in Fig. 2 was obtained from Fourier Transform of the 1D EPI signal time series, obtained by selecting a central voxel from each 2D time frame from the solenoid modulated cylindrical water phantom (voxel size = 2.3 × 2.3 × 5 mm^3). A 1.8 Hz sinusoidal current of 33 μA flowed through the 33 mm diameter circular modulating coil, producing an RMS magnetic field of 7.2×10^{-9} T. The magnetic field from the current was clearly detected (SNR = 45:1), suggesting that it should be possible to measure currents up to a factor of ~20 weaker than this, i.e., $\sim 3 \times 10^{-10}$ T.

The contrast percentage was expressed relative to the full equilibrium signal (i.e. the full voxel magnetization), corrected from the measured signal using T1 = 1600 ms, T2* = 28 ms for the water phantom, measured using a series of repeat times and echo times and the standard formula for the signal from a gradient echo sequence. The magnitude signal modulation of 1.0% (with background noise subtraction) was in reasonable agreement with the predicted value of 0.9% for an echo time of 30 ms and the applied field of 7.2×10^{-9} T. The TSD of the magnitude signal was 0.1% for phantom experiments without the alternating current applied at TE = 30 ms using surface coil acquisition. Fig. 3 shows the percentage modulation of the magnitude images as a function of applied magnetic field strength. The solid line shows the predictions from the linear model for TE = 30 ms as a function of magnetic field strength. The lowest detectable RMS magnetic field measured with the phantom was actually 5.7×10^{-10} T corresponding to 2.7 μA sinusoidal current at an SNR of 2:1. It can be seen that, in the phantom measurements, there was a linear dependence of signal change with modulating field strength. This is similar to the estimates of field from the axons discussed above.

Spectra acquired from the 19 cm cylindrical phantom with and without the strobe light applied showed no evidence of direct electromagnetic interference over the range of frequencies used in the visual stimulation experiments (data not shown for brevity).

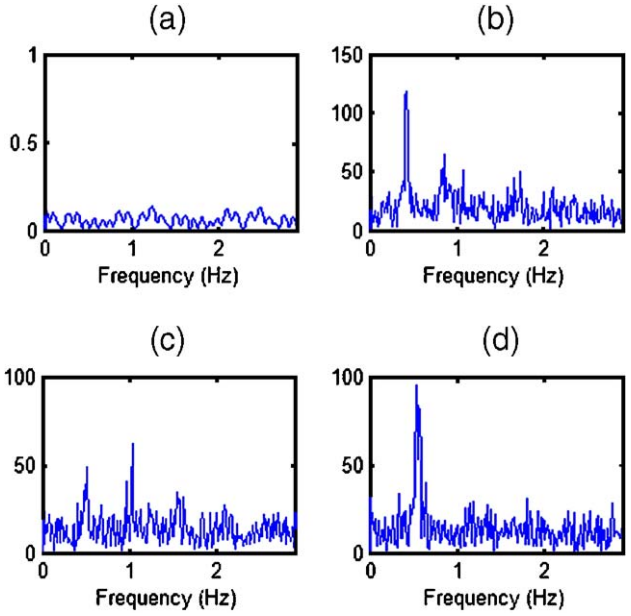

Fig. 4. Experiments to assess motion of the optic nerve. The spectra represent Fourier transforms of the time series of the horizontal coordinate offset (perpendicular to the long axis of the optic nerve) from autocorrelation analysis of selected sub-images containing only the optic nerve for four different cases: (a) 2.5 Hz strobe stimulation, (b) simultaneous 2.5 Hz strobe stimulation and 0.5 Hz deliberate blinking movement, (c) 0.5 Hz deliberate blinking movement, (d) 0.5 Hz deliberate eyeball movement from side to side. The *y* axes are all on the same scale in arbitrary units. It can be seen that, with strobe illumination and no deliberate motion, no spectral peaks corresponding to regular motion are detected, whereas, with deliberate motion, spectral peaks and their harmonics at the motion frequency are easily detected. Any data sets with motion components identified as spectral peaks were rejected.

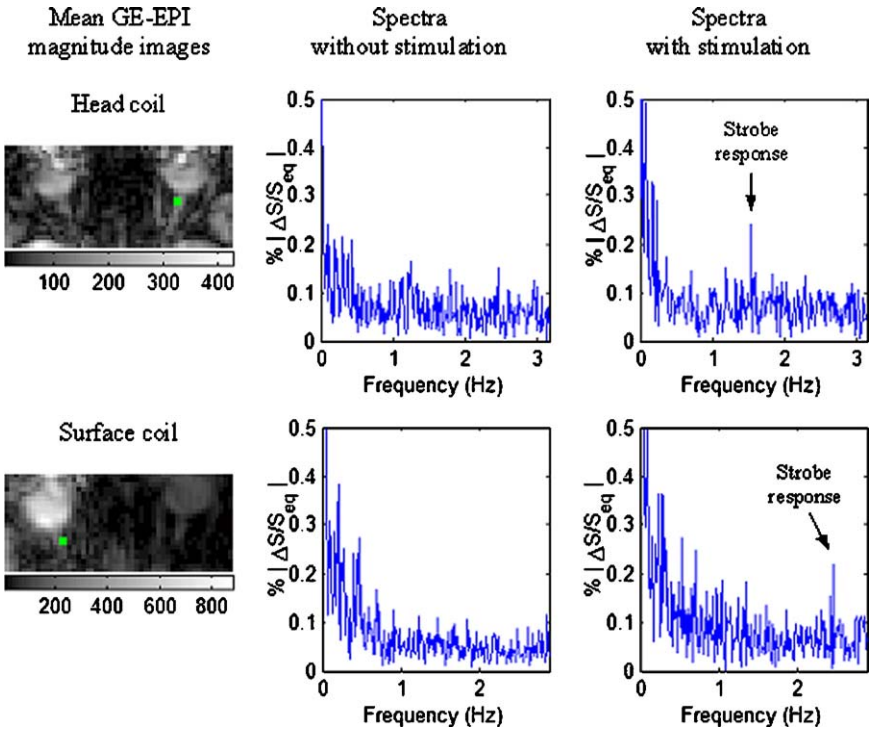

Fig. 5. Typical measured frequency spectra for ROI selected in the optic nerve (2 × 2 voxel ROI, voxel size 1.88 × 1.88 × 5 mm^3) using either a head coil or a surface coil with 1.5 Hz and 2.5 Hz strobe stimulation respectively compared with the control experiment without stimulation. A Student's t test ($P < 0.05$, degree of freedom = 32) showed that spectra with and without stimulation were significantly different.

In vivo experiments

Fig. 4 illustrates the results of 1D Fourier transforming the time series (perpendicular to the optic nerve) obtained from the spatial offsets in the horizontal direction calculated by autocorrelation analysis of an ROI selected around the optic nerve for four different experiments. It can be seen that, in the presence of the strobe stimulation with no deliberate blinking (Fig. 4a), no spectral components were observed at the strobe frequency. This is typical of all data sets used for the analysis reported here. With deliberate blinking or movement of the eyeballs (Figs. 4b–d), spectral components were clearly observed in the spectrum at the frequency of the motion plus harmonics. Any data sets with such motion components at the strobe frequency were rejected. Motion of the optic nerve in the vertical direction (i.e. along the long axis) was always found to be much less than in the horizontal direction as would be expected. Motion analysis is made easier by the regular rectangular structure of the optic nerve in the ROI when fat saturation is applied. All volunteers were reported to be able to generally avoid blinking or deliberate motion during the scans. Occasional involuntary blinking was unavoidable, but the effects of this could be clearly identified in the time series and did not give rise to resolved spectral components.

Fig. 5 shows typical mean 2D GE-EPI magnitude images and 1D frequency spectra of the optic nerve created by Fourier transforming the time series of the mean magnitude signal in an ROI selected in the optic nerve (2 × 2 voxel ROI, voxel size = 1.88 × 1.88 × 5 mm^3). In these examples, the strobe response was detected in the optic nerve at 1.5 Hz (acquired with the head coil) and at 2.5 Hz (acquired with the surface coil in another subject). The observed frequencies were consistent with the two applied strobe light

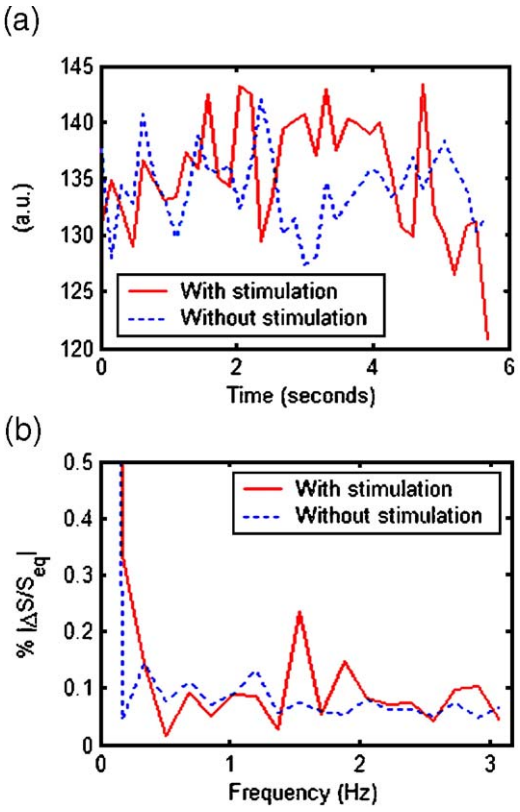

Fig. 6. (a) Unsynchronized averaged time series for data sets containing 9-strobe flashes of 1.5 Hz and the control experiment without stimulation. (b) Fourier transform of the averaged time series in panel a showing the 1.5 Hz strobe response.

frequencies and did not occur in the same ROI without stimulation under dark-adapted control conditions. The contrast percentage was expressed relative to the full equilibrium signal, corrected from the measured signal using T1 = 718 ms (Wansapura et al., 1999) for the optic nerve and the standard formula for the signal from a gradient echo sequence. The amplitude of the response in Fig. 5 for 1.5 Hz was 0.17% and for 2.5 Hz was 0.16% of fully relaxed equilibrium signal with mean background noise adjustment, which was typical of all measured responses, with an SNR ~6:1. This would correspond to a peak field of $\sim 1.2 \times 10^{-9}$ T using the results shown in Fig. 9 (TE = 32.4 ms). This value is generally consistent with estimates of field from MEG and the simple wire model of the axon made earlier, although it should be noted that there are many assumptions made in relating the percentage changes observed to actual field values. Signals from these single, anatomically chosen ROI over a spectral range of ±0.1 Hz centered on the observed response peak were significantly different from control spectra according to a Student's *t* test ($P < 0.05$, degrees of freedom = 32). In the example in Fig. 5, the *t* value for the 1.5 Hz and 2.5 Hz data sets was 2.15 and 2.29 respectively, which are both higher than the tabulated *t* value (2.04) for $P = 0.05$. Peaks due to respiration (~0.25–0.33 Hz) and heartbeat (~1.0–1.4 Hz) were seen in the optic nerve spectra, although these were much weaker than those observed from spectra obtained from ROI located within brain parenchyma, presumably due to lack of major vessels.

The unsynchronized averaged time series in Fig. 6a was taken from the data set in Fig. 5 with 1.5 Hz strobe light stimulation. This experiment used a TR = 158 ms; and each flash had a period of ~667 ms. An interval of 37 time frames would correspond to approximately 9-strobe responses. Fourier transformation on this average time series produced the 1.5 Hz strobe response as shown in Fig. 6b, with a signal change similar to the result found in Fig. 5. The control experiment without stimulation is also shown with the dotted line.

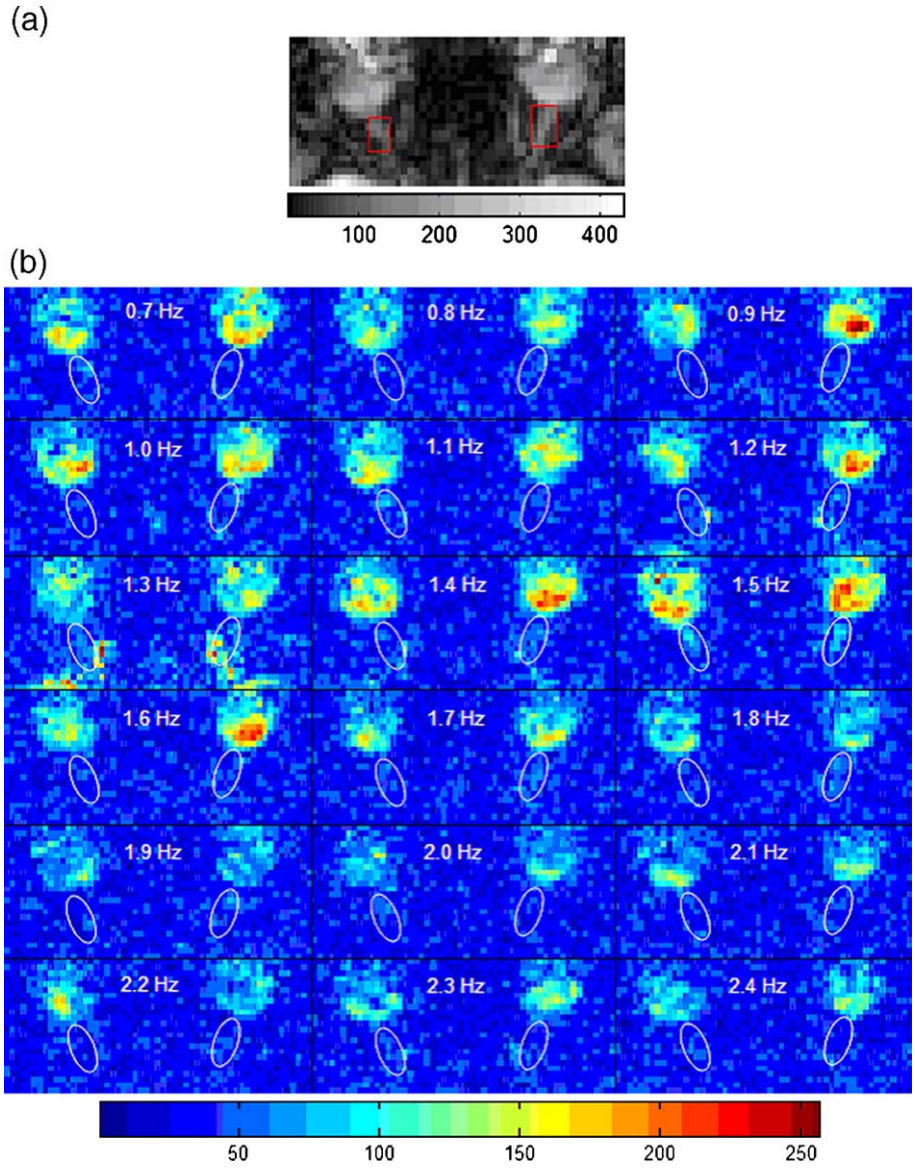

Fig. 7. (a) Mean GE-EPI magnitude image and (b) a range of frequency maps from 0.7 Hz to 2.4 Hz at 0.1 Hz intervals using the head coil showing the eyeballs with the optic nerve positions outlined for 1.5 Hz strobe stimulation of both eyes. Increased signal at the strobe frequency can clearly be seen in both optic nerves.

A mean GE-EPI magnitude image acquired with the head coil from an experiment with 1.5 Hz strobe light stimulation is shown in Fig. 7a, with the calculated frequency maps in Fig. 7b ranging from 0.7 Hz to 2.4 Hz in 0.1 Hz steps. The optic nerves are most clearly defined within their oval markers at the strobe frequency, suggesting direct detection of the modulation caused by the axonal currents. It was also found that many pixels in the eyeballs were highlighted in most of the frequency ranges, especially in the region of the retina. The heartbeat was measured between 1.2 and 1.3 Hz in this experiment. A pixel-by-pixel Student's t test ($P < 0.05$, degrees of freedom = 90, corrected $P < 0.001$) for the 1.5 Hz map between data sets with and without stimulation for the optic nerves ROI (as shown within the rectangular ROI in Fig. 7a) was significantly different with a t value of 6.22, which is much higher than the tabulated t value (3.4) for $P = 0.001$. The probability of equality between data sets with and without stimulation was 2×10^{-8}.

Fig. 8 shows mean GE-EPI magnitude images (gray scale) and frequency maps (color scale) obtained with 1.5 Hz strobe stimulation. Magnitude images are shown for comparison. The regions corresponding to the optic nerves within the oval markers generally showed a greater response when one or both eyes were being strobe stimulated, compared to the control experiments without stimulation (open or closed eyes). Fig. 9 shows in vivo data acquired at different stimulation frequencies at echo times between 30 ms and 40 ms in three subjects plotted on the theoretical curve for the linear model (the results for TE = 50 ms and 78 ms were not statistically significant but followed a linear trend).

Table 2 summarizes all the experiments that achieved statistical significance using GE-EPI magnitude images performed over the range of stimulation frequencies (0.7–3.3 Hz). Table 3 summarizes all the experiments acquired with complex data, which were used for offline reconstruction of magnitude and phase images. There were 30 out of 52 experiments (using magnitude images; without motion) with detected strobe responses and which showed significant difference of the optic nerve ROI in the strobe frequency maps between data sets with and without stimulation, according to a Student's t test with Bonferroni correction of the P value according to the number of voxels used for the t test. This represents a 58% success rate in detecting significant strobe responses in the optic nerve. It was found that 7 experiments had motion in the optic nerves. The mean magnitude signal change and standard deviation were (0.15 ± 0.05)% for all experiments using TE = 32.4 ms. The mean predicted field was (1.2 ± 0.4) nT according to the Lorentzian field simulation in Fig. 9, with a mean SNR = 4:1.

Discussion

The entire process of vision is transmitted through the two optic nerves. Visual stimulation gives rise to an ionic current flow from action potentials in the axons of the optic nerve, which produces a pulsating magnetic field that can modulate the MR signal. In these experiments, a mean spectral response of (0.15 ± 0.05)% relative to the full equilibrium magnitude signal for TE = 32.4 ms was

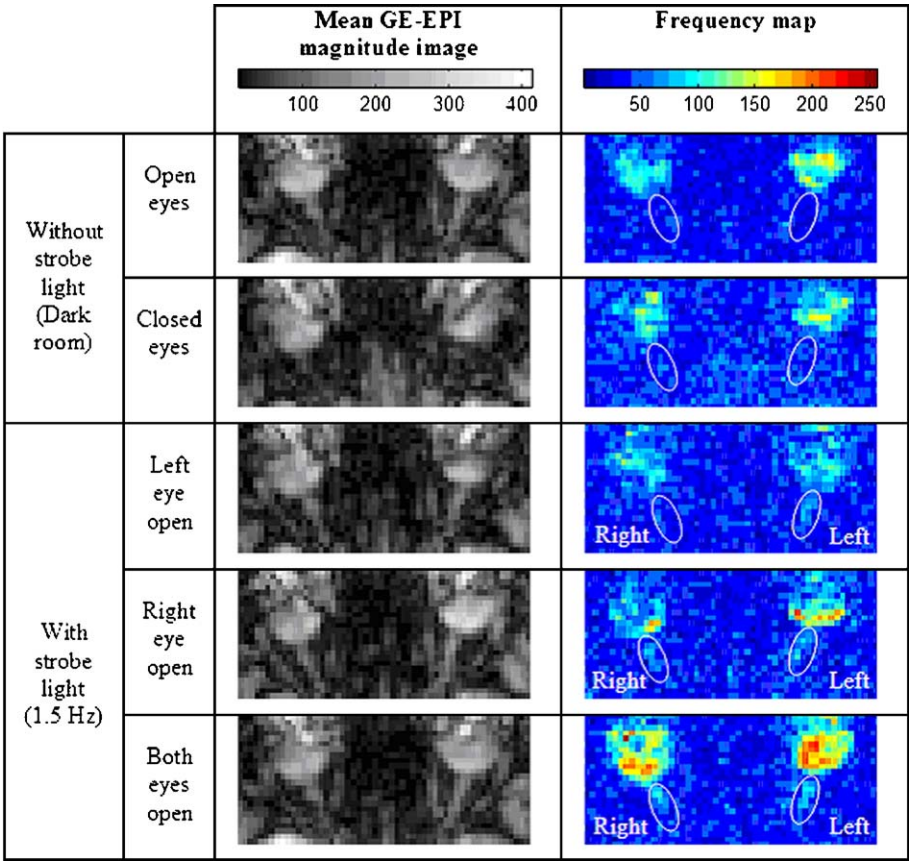

Fig. 8. Frequency maps calculated at 1.5 Hz strobe stimulation obtained with the head coil. The optic nerve regions are outlined for comparison with the experiments acquired with either open or closed eyes.

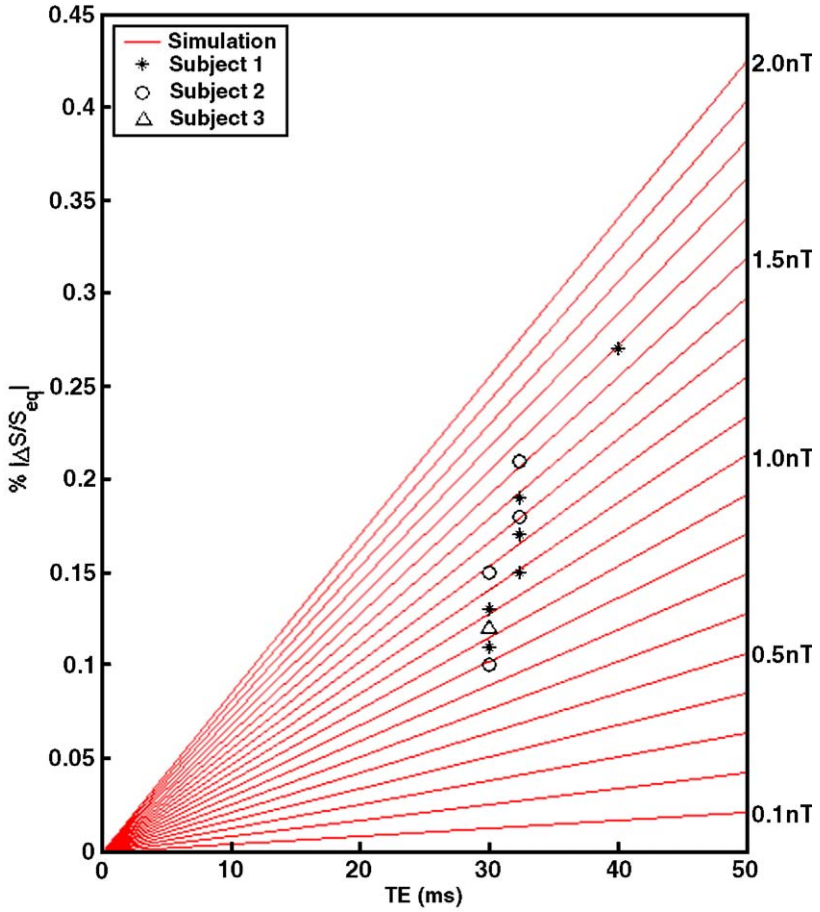

Fig. 9. In vivo percentage signal changes with respect to the fully relaxed equilibrium signal for data acquired at TE = 30, 32.4 and 40 ms plotted on the linear theoretical curve for different strobe stimulation frequencies (three different subjects). Experiments were also performed at TE = 50 ms and 78 ms, but the responses did not reach statistical significance. The simulation was plotted for a range of fields from 1.0×10^{-10} T to 2.0×10^{-9} T in 10^{-10} T steps with each line corresponding to the percentage changes for a particular constant field value (as shown on the right hand axis) as a function of echo time.

observed at the strobe frequency from the optic nerve, corresponding to an estimated field of (1.2 ± 0.4) nT, as assessed from the predictions of Fig. 9, and by comparison with the calibrated phantom measurements. The error in field is estimated from the standard deviation of the mean spectral response and is similar to the minimum detected field measured using phantoms. The mean measured signal change as a function of echo time is consistent with a linear model but is somewhat larger than has been suggested from MEG studies for evoked sources.

The individual action potentials are predicted to flow through the image voxel in about 300 μs and so can be thought of as being instantaneous from the viewpoint of the experiments presented here. This 'residence time' may be an accessible and interesting parameter to measure in the future and should be accounted for in modeling studies. However, the overall action potential burst from the retina is expected to last for several hundred milliseconds, which provides sufficient time to create significant intravoxel dephasing during the acquisition. As action potentials are effectively 'digital' and typically generate the same current, unless bursting very rapidly,

Table 2
Number of in vivo experiments using GE-EPI magnitude images

Strobe frequency (Hz)	Detected	Not detected
0.7	–	1
1.3	–	1
1.5	3	1
1.6	5	5
1.7	5	3
1.8	4	–
1.9	1	–
2.0	1	–
2.2	–	1
2.4	1	3
2.5	2	1
3.0	1	–
3.3	1	–
Total	24	16

Table 3
Number of in vivo experiments acquired with complex data

Strobe frequency (Hz)	Magnitude images		Phase images	
	Detected	Not detected	Detected	Not detected
0.7	–	1	–	1
0.9	–	1	–	1
1.5	1	1	–	2
1.7	1	2	–	3
1.9	2	1	–	3
2.4	2	–	1	1
Total	6	6	1	11

the magnitude of response should be similar from all volunteers as observed in this study given a similar stimulation paradigm and similar recruitment of number of axons. The spectral response measured from the optic nerve appears to be largely free of the cardiac and respiratory 'artifacts' seen in other areas of the brain such as the visual cortex, presumably due to lack of major vessels, hence, it is easier to observe changes due to stimuli.

A comprehensive review of blood flow and hemodynamic response in the optic nerve and retina of animals and humans was recently provided by Riva et al. (2005). Flow and oxygenation changes in the optic nerve vessels which serve the retina and choroid plexus could possibly produce a BOLD-like response in the optic nerve, although the detailed form of the response may be different to that found in the cortex. However, some of the vessels serving the retina arrive directly through the retro-orbital fat rather than through the optic nerve. Duong et al. (2002) showed an fMRI response of about 1% in the cat retina at 9.4 T, a field strength where large BOLD effects of, typically, 5–10% are found from the cortex. Correspondingly, weaker effects would be expected at the field strength of 1.5 T used in this study where maximum BOLD signal changes in the cortex are only about 1%. The maximum positive BOLD signal occurs between 6 and 10 s in humans which means the maximum of the frequency response occurs at around 0.1 Hz, much lower than the frequencies used in this study. A fast initial negative BOLD response has been reported in some studies with a maximum amplitude of ~0.1–0.4% after about 3 s or at a frequency of 0.33 Hz (Shmuel et al., 2002). At the faster stimulus frequencies used in this study of 0.7–3.3 Hz, the effect should be even smaller (<0.1%). This fast 'early dip' effect is thought to be due to direct oxygen consumption by neurons (Shmuel et al., 2002; Vazquez and Noll, 1998) and might provide a response at the relatively fast stimulus frequencies used and so cannot be totally ruled out as an explanation of the observed effects. If this is the case, then these measurements would alternatively provide the first report of such a fast response in the optic nerve. However, veins in the optic nerve occupy a small volume fraction (1–5%) compared to the axons, and the lack of dominant spectral peaks at the cardiac frequency in the spectra measured here suggests that the effects of the vasculature are weak in the optic nerve.

The axons from the retina are believed to carry current unidirectionally from the retina towards the brain. The probability of any possible 'retrograde' currents being sufficiently large in amplitude and of the correct phase to cancel the field generated on stimulation is thus thought to be very low.

The eyes are of course very mobile, which can potentially lead to stimulus-related motion artifacts. Care was taken to minimize any effects of such motion by training the volunteers not to move their eyes or blink during the relatively short duration of the study. Regular, rapid saccadic motion of the eyes would be expected at a frequency around 3 Hz, which was only detected in one subject out of five. Autocorrelation analysis was used to assess global and local motion between successive image frames, and any data sets with significant motion were rejected. Furthermore, artifacts induced by deliberate blinking or motion of the eyes produced broader spectral peaks than those at the stimulus-related frequencies, as expected for rapid, short duration motions. Strobe responses were observed with phase encoding in either left–right or anterior–posterior directions which also helps remove concerns about motion artifacts. Spectral components were observed across all measured frequencies in the eyeballs, although these were most pronounced in the retinal region close to the stimulation frequency (1.4–1.6 Hz for the experiment shown in Fig. 7). Contributions from currents generated during 'photo-processing' and 'analogue to digital conversion' in the retina are present during visual stimulation and in many of the frequency maps, the retinal regions gave the most significantly activated pixels. However, it is more difficult to detect rotational motion of the eyeball due to the circular shape, and there is also a possibility that eddy currents from the applied gradients may be set up in the vitreous humor.

There have been a number of previous studies aimed at detecting the effects of currents expected from neuronal sources on the magnetic resonance signal both in phantoms and in vivo. Kamei et al. used a subtraction method with alternating gradient polarity to investigate neuronal current distribution and detected a dipole of 90 nAm in phantoms at 6.3 T and also investigated a motor task in vivo at 1.5 T using EPI (Kamei et al., 1999), but this study has not yet been replicated. Bodurka et al. detected magnetic field changes of 2×10^{-10} T in phase images of a water phantom due to current flow in a wire, using a single-shot spin-echo (SE) echo planar imaging (EPI) phase mapping sequence (Bodurka et al., 1999). Konn et al. detected the effects of a field strength of 1.1×10^{-10} T in EPI phase images of a phantom, where the neuronal current flow was modeled as an extended current dipole located in a conducting sphere (Konn et al., 2003). The ghost reconstructed alternating current estimation (GRACE) method, introduced by Yang et al. (2003), estimated alternating current amplitudes using ghost images created when the magnetic field from a fluctuating current modulated the phase between successive phase-encode views of a conventional gradient echo sequence, allowing a frequency response governed by 1/TR. Subsequently, magnetic fields as low as 4×10^{-10} T, with frequencies as high as 90 Hz, have been detected using sequentially averaged GRACE in phantoms (Chow et al., 2004).

Xiong et al. have claimed to detect magnetic fields in vivo using magnitude only measurements and a visuo-motor paradigm. They suggested that magnitude rather than phase images should be more sensitive due to intravoxel phase cancellation resulting in zero signal in phase images for a symmetrical distribution of sources (Xiong et al., 2003). Effects of up to 1% were observed in the magnitude images, which was in line with their predictions based on a quadratic dependence of signal on TE. However, no details of their quadratic model have yet been published. Their study used very long echo times (up to 100 ms) to allow for a long phase integration, potentially increasing sensitivity but also creating echo planar images highly prone to distortion and phase accumulation errors due, for example, to residual eddy currents. The images used to calculate their time series data were acquired with long TR (1000 ms) and synthesized retrospectively from six successive runs acquired at approximately 2 min intervals. This makes the time series very vulnerable to motion artifact and slow scanner drifts and, as such, not really suited to measuring waveforms and correlations from real-time processes occurring in the tens of milliseconds range. A recent study by Parkes et al. to replicate this work failed to detect effects of direct neuronal activity (Parkes et al., 2005).

Konn et al. have attempted to detect alpha waves in the brain at frequencies between 8.5 and 13 Hz, which are thought to result from dipole moments ten times higher than those of evoked potentials (~100 nAm compared to ~10 nAm respectively as measured using MEG) using phase images (Konn et al., 2003; Konn et al., 2004). MR results were compared with EEG obtained

using the same paradigm including simulated scanner acoustic noise outside the magnet, although it was not possible to independently test whether alpha waves were actually present within the magnet environment during this study. Furthermore, the volume contributing to the dipole moment was unknown, so the 100 nAm dipole strength could correspond to a weak local peak magnetic field through an extended volume, as might be expected for distributed alpha waves. The authors suggest that phase images should have several orders of magnitude higher contrast to noise ratio than magnitude images for detection of weak dipolar fields (<100 nAm) but only for dipole sources which are asymmetric with respect to the imaging voxel. This may be the case for alpha waves which are distributed over extended volumes, but effects in phase images are unlikely for the highly aligned and symmetrically distributed axons of the optic nerve. Only one significant response to the strobe stimulation was seen in the twelve in vivo phase images acquired in this study, which may thus be a chance result. Further experimental and simulation studies are required to assess the relative merits of magnitude versus phase images for realistic distributions of magnetic sources.

Liston et al. (2004) retrospectively analyzed data acquired as part of an fMRI study to assess the possibility of large spiking currents (finite impulse responses (FIRs)) associated with seizures in epilepsy patients. This study showed possible evidence for detection of generalized spike wave discharge (GSWD) complexes which are thought to be at least twenty times larger than evoked responses, based on EEG voltage measurements. However, the study was performed with a long TR of 3000 ms, and so the signal time courses were subject to aliasing of the 3 Hz bursts which fell between rebinned slice locations.

Chu et al. (2004) used a binary 'm-series' visual stimulation paradigm to simultaneously measure the slow BOLD response and any possible rapid changes due to direct neuronal effects. They compared their results with MEG which easily detected the m-series stimulation BOLD-related changes but found no evidence of effects due to neuronal firing in either phase or magnitude MR data. The m-series paradigm does not produce excitation at a well-defined frequency but effectively spreads excitation over a range of frequencies, which would perhaps make detection less likely. The complex stimulation paradigm uses a two-stage correlation analysis and also assumes linearity of the BOLD process which has been previously shown to become slightly non-linear for short stimulus durations (Vazquez and Noll, 1998). The rapidly changing non-periodic stimulus may also lead to complicated transient approach to steady state effects which could further complicate interpretation of the signal response, although phase spoiling was employed to reduce these effects.

Petridou et al. recently performed an elegant set of MR experiments in a rat cell culture at 7 T in a planar configuration which showed spontaneous electrical activity as detected by a set of surrounding electrodes and which could simultaneously be detected by magnetic modulation in both magnitude and phase spectra (Petridou et al.,2005). The electrical activity was terminated on introduction of a cell toxin (tetrodotoxin) to the preparation and difference spectra formed. The phase spectra provided a more clear demonstration of the activity than the magnitude spectra in this study.

The ability to detect an effect in the optic nerve is thought to depend on stimulating synchronous firing of a large number of axons over an extended duration to allow intravoxel dephasing to occur. Recruitment of the more numerous rods as well as the cones is believed to be critical in this respect, which is encouraged by dark adaptation of the subject prior to the experiment. ERG data show that retinal output in response to a single short flash can last for several hundred milliseconds (Shimada et al., 2001). Assuming this nerve burst repeats with the strobe frequency, the expected spectrum would be the Fourier transform of the burst sampled at harmonics of the strobe frequency. The 1D time series used in the Fourier spectral analysis essentially samples the burst at an interval of TR down the time frames, and therefore the spectrum will be aliased if it is wider than 1/TR. Clearly, the shorter the nerve impulse burst, then the wider the spectrum and the more likely aliasing is to occur. Individual action potentials lasting for only ~1 ms would produce a very broad spectral response and so may not be detected since their aliased harmonics could be buried in noise since there is less energy in a short pulse. In this work, we have focused on detecting the fundamental frequency component of the longer nerve burst envelope from hundreds of thousands of axons expected in response to strobe stimulation, but even detection of aliased components would be significant in suggesting an axonal field effect.

Improved time-dependent simulations of axonal firing in the optic nerve may help understand the details of the sensitivity of MRI to these magnetic modulation processes. Certainly, if motion effects can be adequately controlled, the optic nerve provides an almost unique possibility within the human body to study intravoxel dephasing effects with external control of both the spatial and temporal modulation of the magnetic sources. Future studies are planned to corroborate this preliminary data with improved detection sensitivity at higher field, with dedicated array coils, with use of contrast agents including dynamically or externally polarized nuclei, with more sophisticated stimuli, with better motion monitoring and control, with increased frequency range as offered by, e.g. the GRACE technique (Yang et al., 2003) and by investigation of other accessible cranial nerve fiber bundles.

Conclusion

This study shows preliminary evidence for detection of a weak perturbation, (0.15 ± 0.05)% of the equilibrium MR signal acquired at 1.5 T from the optic nerve of dark-adapted adult human subjects which is consistent in amplitude and frequency with the expected magnetic fields from synchronized and extended action potential bursts in axons of the optic nerve due to repetitive strobe light stimulation in the range 0.7–3.3 Hz. The effect may also be consistent with a very fast residual component of the BOLD response, however, this is thought to be less likely at the higher stimulus frequencies used in this study. Further work is required to confirm these preliminary findings.

Acknowledgments

We would like to acknowledge Dr. James M. Wild, Dr. Kuan J. Lee, Prof. Paul D. Griffiths and Prof. Ian R. Young for stimulating discussions. We would also like to thank Prof. Richard Bowtell, Prof. Penny Gowland and their PhD students at the Sir Peter Mansfield MR Centre, University of Nottingham for freely sharing their ideas on direct neuronal detection by MR.

References

Barber, D.C., Brown, B.H., 1983. Imaging spatial distributions of resistivity using applied potential tomography. Electron. Lett. 19, 933–935.

Bodurka, J., Bandettini, P.A., 2002. Toward direct mapping of neuronal activity: MRI detection of ultraweak, transient magnetic field changes. Magn. Reson. Med. 47, 1052–1058.

Bodurka, J., Jesmanowicz, A., Hyde, J.S., Xu, H., Estkowski, L., Li, S., 1999. Current-induced magnetic resonance phase imaging. Magn. Reson. Imaging 137, 265–271.

Brown, R.J.S., 1961. Distribution of fields from randomly placed dipoles: free precession signal decay as result of magnetic grains. Phys. Rev. 121, 1379–1383.

Chow, L.S., Cook, G., Paley, M.N.J., 2004. Attempting to detect firing of the optic nerve using GRACE MR and sequential averaging. Proc. UK Radiological Congress, p. 24.

Chu, R., deZwart, J., van Gelderen, P., Fukunaga, M., Kellman, P., Holroyd, T., Duyn, J.H., 2004. Hunting for neuronal currents: absence of rapid MRI signal changes during visual evoked response. NeuroImage 23, 1059–1067.

Duong, T.Q., Ngan, S.C., Ugurbil, K., Kim, S.G., 2002. Functional magnetic resonance imaging of the retina. Invest. Ophthalmol. Visual Sci. 43, 1176–1181.

Hamalainen, M., Hari, R., Ilmoniemi, R.J., Knuutila, J., Lounasmaa, O.V., 1993. Magnetoencephalography—Theory, instrumentation, and applications to non-invasive studies of the working human brain. Rev. Mod. Phys. 65, 413–497.

Hennig, J., Speck, O., Koch, M.A., Weiller, C., 2003. Functional magnetic resonance imaging: a review of methodological aspects and clinical applications. Magn. Reson. Imaging 18, 1–15.

Josephs, O., Henson, R.N., 1999. Event-related functional magnetic resonance imaging: modelling, inference and optimization. Philos. Trans. R. Soc. Lond., Ser. B Biol. Sci. 29 (354(1387)), 1215–1228.

Joy, M., Scott, G., Henkelman, M., 1989. In vivo detection of applied electric currents by magnetic resonance imaging. Magn. Reson. Imaging 7, 89–94.

Kamei, H.I.K., Yshikawa, K., Ueno, S., 1999. Neuronal current distribution imaging using magnetic resonance. IEEE Trans. Magn. 35, 4109–4111.

Kandel, E.R., Schwartz, J.H., Jessell, T.M., 2000. Principles of Neural Science, 4th Edition. McGraw-Hill, New York.

Kennan, R.P., Zhong, H., Gore, J.C., 1994. Intrasvascular susceptibility contrast mechanisms in tissues. Magn. Reson. Med. 31, 9–21.

Kolb, H., Fernandez, E., Nelson, R., 2002. The Organization of the Retina and the Visual System (http://webvision.med.utah.edu).

Konn, D., 2003. Direct detection of neuronal activity in the brain using MRI. University of Nottingham, PhD thesis.

Konn, D., Gowland, P., Bowtell, R., 2003. MRI detection of weak magnetic fields due to an extended current dipole in a conducting sphere: a model for direct detection of neuronal currents in the brain. Magn. Reson. Med. 50, 40–49.

Konn, D., Gowland, P., Bowtell, R., 2004. Initial attempts at directly detecting alpha wave activity in the brain using MRI. Magn. Reson. Imag. 22, 1413–1427.

Liston, A.D., Salek-Haddadi, A., Kiebel, S.J., Hamandi, K., Turner, R., Lemieux, L., 2004. The MR detection of neuronal depolarization during 3-Hz spike-and-wave complexes in generalized epilepsy. Magn. Reson. Imaging 22, 1441–1444.

Logothethis, N.K., Pauls, J., Augath, M., Trinath, T., Oeltermann, A., 2001. Neurophysiological investigation of the basis of the fMRI signal. Nature 412, 150–157.

Mikelberg, F.S., Drance, S.M., Schulzer, M., Yidegiligne, H.M., Weis, M.M., 1989. The normal human optic nerve. Axon count and axon diameter distribution. Ophthalmology 96, 1325–1328.

Nolte, J., 2002. The Human Brain—An Introduction to Its Functional Anatomy, 5th Edition. St. Louise Mo. Mosby.

Ogawa, S., Lee, T.M., Nayak, A.S., Glynn, P., 1990. Oxygenation-sensitive contrast in magnetic resonance image of rodent brain at high magnetic fields. Magn. Reson. Med. 14, 68–78.

Purves, D., Augustine, G.J., Fitzpatrick, D., Katz, L.C., LaMantia, A.S., McNamara, J.O., Williams, S.M., 2001. Neuroscience, 2nd edition. Sinauer Associates Inc., Sunderland, MA. Chap. 4.

Parkes, L.M., Lange, F., Norris, D.G., Fries, P., Toni, I., 2005. Failure to replicate the direct detection of magnetic field changes associated with neuronal activity. Proc. 11th Annual Meeting of British Chapter, p. 20.

Petridou, N., Silva, A.C., Plenz, D., Bodurka, J., Bandettini, P., 2005. Direct MR detection of neuronal activity in vitro at 7 T. Proc Int. Soc. Mag. Res. In Medn., 13.

Raichle, M.E., 2001. Bold insights. Nature 412, 128–130.

Riva, C.E., Logean, E., Flasini, B., 2005. Visually evoked hemodynamical response and assessment of neurovascular coupling in the optic nerve and retina. Prog. Retinal Eye Res. 24, 183–215.

Scott, G.C., Joy, M.L.G., Armstrong, R.L., Henkelman, R.M., 1995. Rotating frame current density imaging. Magn. Reson. Med. 33, 355–369.

Scott, G.C., Joy, M.L.G., Armstrong, R.L., Henkelman, R.M., 1992. Sensitivity of magnetic resonance current density imaging. JMR 97, 235–254.

Shmuel, A., Yacoub, E., Pfeuffer, J., Van de Moortele, P.F., Adriany, G., Hu, X., Ugurbil, K., 2002. Sustained negative BOLD, blood flow and oxygen consumption response and its coupling to the positive response in the human brain. Neuron 36, 195–210.

Shimada, Y., Li, Y., Bearse Jr., M.A., Sutter, E.E., Fung, W., 2001. Assessment of early retinal changes in diabetes using a new multifocal ERG protocol. J. Ophthalmol. 85, 414–419.

Sterling, P., Demb, J., 2004. The Synaptic Organization of the Brain. In: Shepherd, G.M. (Ed.), Retina. Oxford Univ. Press, New York. Review.

Vazquez, A.L., Noll, D.C., 1998. Nonlinear aspects of the BOLD response in functional MRI. NeuroImage 7, 108–118.

Wansapura, J.P., Holland, S.K., Dunn, R.S., Ball Jr., W.S., 1999. NMR relaxation times in the human brain at 3.0 Tesla. J. Magn. Reson. Imaging 9, 531–538.

Wheeler-Kingshott, C.A., Parker, G.J., Symms, M.R., Hickman, S.J., Tofts, P.S., Miller, D.H., Barker, G.J., 2002. ADC mapping of the human optic nerve: increased resolution, coverage, and reliability with CSF-suppressed ZOOM-EPI. Magn. Reson. Med. 47, 24–31.

Xiong, J., Fox, P.T., Gao, J., 2003. Directly mapping magnetic field effects of neuronal activity by magnetic resonance imaging. Hum. Brain Mapp. 20, 41–49.

Yang, H., Cook, G.G., Paley, M.N.J., 2003. Mapping of periodic waveforms using the ghost reconstructed alternating current estimation (GRACE) magnetic resonance imaging technique. Magn. Reson. Med. 50, 633–637.